THE JOURNAL OF BIOLOGICAL CHEMISTRY
Vol. 279, No. 49, Issue of December 3, pp. 51193–51202, 2004
Printed in U.S.A.

The H^+-pyrophosphatase of *Rhodospirillum rubrum* Is Predominantly Located in Polyphosphate-rich Acidocalcisomes*[S]

Received for publication, June 2, 2004, and in revised form, September 9, 2004
Published, JBC Papers in Press, September 15, 2004, DOI 10.1074/jbc.M406099200

Manfredo Seufferheld‡, Christopher R. Lea§, Mauricio Vieira‡, Eric Oldfield§, and Roberto Docampo‡¶

From the ‡Laboratory of Molecular Parasitology, Department of Pathobiology and Center for Zoonoses Research, University of Illinois at Urbana-Champaign, Urbana, Illinois 61802 and the §Department of Chemistry, University of Illinois at Urbana-Champaign, Urbana, Illinois 61801

Acidocalcisomes are acidic, calcium storage compartments with a H^+ pump located in their membrane that have been described in several unicellular eukaryotes, including trypanosomatid and apicomplexan parasites, algae, and slime molds, and have also been found in the bacterium *Agrobacterium tumefaciens*. In this work, we report that the H^+-pyrophosphatase (H^+-PPase) of *Rhodospirillum rubrum*, the first enzyme of this type that was identified and thought to be localized only to chromatophore membranes, is predominantly located in acidocalcisomes. The identification of the acidocalcisomes of *R. rubrum* was carried out by using transmission electron microscopy, x-ray microanalysis, and immunofluorescence microscopy. Purification of acidocalcisomes using iodixanol gradients indicated co-localization of the H^+-PPase with pyrophosphate (PP_i) and short and long chain polyphosphates (polyPs) but a lack of markers of the plasma membrane. polyP was also localized to the acidocalcisomes by using 4′,6′-diamino-2-phenylindole staining and identified by using ^{31}P NMR and biochemical methods. Calcium in the acidocalcisomes increased when the bacteria were incubated at high extracellular calcium concentrations. The number of acidocalcisomes and chromatophore membranes as well as the amounts of PP_i and polyP increased when bacteria were grown in the light. Taken together, these results suggest that the H^+-PPase of *R. rubrum* has two distinct roles depending on its location acting as an intracellular proton pump in acidocalcisomes but in PP_i synthesis in the chromatophore membranes.

Membrane-bound H^+-pyrophosphatases (H^+-PPases)[1] have been found in various organelles. Mitochondria possess an H^+-PPase that may be dimeric (1) and that is oriented in such a way as to pump protons out into the cytosol (2, 3). Vacuoles from plants as well as those from charophyte algae and *Acetabularia* have a monomeric H^+-PPase that functions to acidify them (4, 5). Acidocalcisomes of trypanosomatid and Apicomplexan parasites (6), as well as from the green alga *Chlamydomonas reinhardtii* (7), the slime mold *Dictyostelium discoideum* (8), and the bacterium *Agrobacterium tumefaciens* (9) also possess an H^+-PPase that is responsible for their acidification. An H^+-PPase is also present in the chromatophores (10, 11). H^+-PPases may also be present in the plasma membranes of some plant cells (12, 13), as well as unicellular eukaryotes (14). The H^+-PPase from the phototrophic bacterium *Rhodospirillum rubrum* was the first H^+-PPase discovered (10, 11). This enzyme is unique in that it catalyzes not only the hydrolysis of PP_i but also the synthesis of PP_i in the light (15). Synthesis is driven by the energy derived from the electrochemical H^+ gradient generated across the membrane of the chromatophores during illumination (15).

Acidocalcisomes have recently been found (9) to be morphologically similar to the volutin granules described in bacteria (16). Volutin or metachromatic granules were the first subcellular entities to be recognized in bacteria (16, 17). Because *R. rubrum* is known to possess volutin granules that accumulate PP_i under illumination (18), we investigated whether the H^+-PPase was also present in these organelles. In this report, we describe the isolation and biochemical properties of the acidocalcisomes of *R. rubrum* and show that, as with the acidocalcisomes of *A. tumefaciens* (9), they are surrounded by a membrane, are acidic because of the presence of the H^+-PPase in their membrane, are rich in PP_i and polyP, and are able to accumulate calcium and other elements. The number of acidocalcisomes as well as the amount of PP_i and polyP significantly increase when the bacteria are grown in light. We also demonstrate that the H^+-PPase is predominantly located in the acidocalcisomes of *R. rubrum*.

EXPERIMENTAL PROCEDURES

Cell Cultures—*R. rubrum* cells (strain Esmarch, Molisch ATCC 17031) were obtained from the American Type Culture Collection. The cells were grown in liquid Sistrom succinate medium (19) with agitation (160 rpm) in the dark or anaerobically in the light (an intensity of 80 μM photons/$m^2 \times s^{-1}$) at 30 °C. The cells were cultured for 4 days and harvested at the stationary phase.

Chemicals—Dulbecco's PBS and reagents for marker enzyme assays were purchased from Sigma. Silicon carbide (400 mesh) was bought from Aldrich. Iodixanol (40% solution; OptiPrep; Nycomed) was obtained from Invitrogen. Benzonase® was from Novagen (Wisconsin, MD). Cycloprodigiosin was a gift from Prof. Hajime Hirata (Himeji Institute of Technology, Hyogo, Japan). Polyclonal antibodies raised against a keyhole limpet hemocyanin-conjugated synthetic peptide corresponding to the hydrophilic loop XII (antibody PAB_{HK} or 326) of plant V-H^+-PPase (20) were kindly provided by Prof. Philip Rea (University of Pennsylvania, Philadelphia, PA). Aminomethylenediphosphonate (AMDP) was synthesized by Michael Martin (Department of Chemistry, University of Illinois at Urbana-Champaign). Monoclonal antibody

* This work was supported in part by National Institutes of Health Grants AI23259 (to R. D.) and GM50694 (to E. O.) and by funds from the Illinois Governor Venture Technology Fund (to R. D.). The costs of publication of this article were defrayed in part by the payment of page charges. This article must therefore be hereby marked "*advertisement*" in accordance with 18 U.S.C. Section 1734 solely to indicate this fact.

[S] The on-line version of this article (available at http://www.jbc.org) contains a supplemental movie.

¶ To whom correspondence should be addressed: Laboratory of Molecular Parasitology, Dept. of Pathobiology and Center for Zoonoses Research, University of Illinois at Urbana-Champaign, 2001 South Lincoln Ave., Urbana, IL 61802. Tel.: 217-333-3845; Fax: 217-244-7421; E-mail: rodoc@uiuc.edu.

[1] The abbreviations used are: H^+-PPase, H^+-pyrophosphatase; polyP, polyphosphate; PP_i, pyrophosphate; PBS, phosphate-buffered saline; AMDP, aminomethylenediphosphonate; DAPI, 4′,6′-diamino-2-phenylindole; DCCD, dicyclohexylcarbo-diimide.

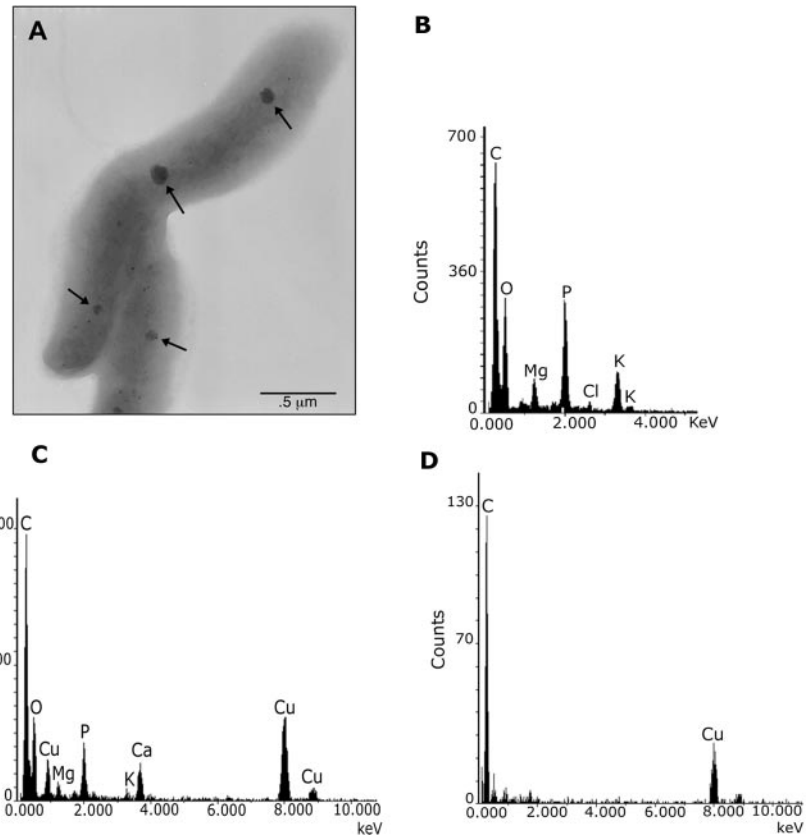

FIG. 1. **Electron microscopy and x-ray microanalysis of whole *R. rubrum*.** *A*, visualization of acidocalcisomes in whole unfixed cells allowed to adhere to a Formvar- and carbon-coated grid and then observed in the transmission electron microscope. Large granules appear located at bending sites and smaller granules of varying sizes appear distributed in the cytosol (*arrows*). *Bar*, 0.5 µm. *B*, x-ray microanalysis of acidocalcisomes in whole cells. *C*, x-ray microanalysis of bacteria grown in calcium-rich medium. *D*, x-ray microanalysis of the background.

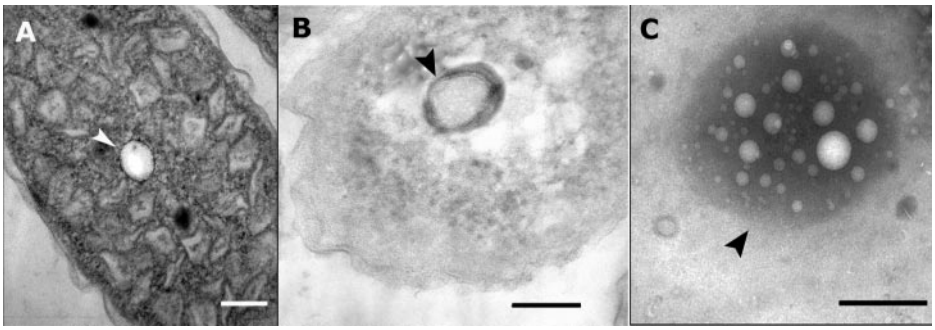

FIG. 2. **Ultrastructure of acidocalcisomes of *R. rubrum*.** Electron micrographs of intact bacteria. The cells were fixed as described under "Experimental Procedures." The *arrowheads* show vacuoles, some containing an electron-dense material in the periphery (*A*) and some occupied by sponge-like electron-dense material (*C*). A membrane is clearly seen enclosing the vacuoles (*arrowhead* in *B*). Chomatophores are seen in the cytoplasm of cells grown under illumination (*A*). *Bars*, 0.12 µm (*A*); 0.15 µm (*B*); 0.1 µm (*C*).

against a keyhole limpet hemocyanin-conjugated synthetic peptide corresponding to the hydrophilic loop XII of *Trypanosoma cruzi* H^+-PPase (21) was prepared at the University of Illinois Biotechnology Center. Molecular weight markers and Coomassie Blue protein assay reagent were from Bio-Rad. EnzChek phosphate assay kit and LysoSensor blue DND-167 (9,10-bis (*N*-morpholinomethyl) anthracene) were from Molecular Probes (Eugene, OR). Prof. Arthur Kornberg (Stanford University School of Medicine, Stanford, CA), kindly provided *Escherichia coli* strain CA38 pTrcPPX1. Prof. Mary Lynne Perille Collins (University of Wisconsin, Milwaukee, WI) provided a polyclonal antibody raised against crude membranes of phototrophic *R. rubrum* cells. All other reagents were of analytical grade.

Isolation of Acidocalcisomes—Bacteria were collected by centrifugation at 3,900 × *g*, and the pellet was resuspended in lysis buffer (125 mM sucrose, 50 mM KCl, 4 mM $MgCl_2$, 0.5 mM EDTA, 20 mM K-Hepes, 5 mM dithiothreitol, 0.1 mM 4-(2-aminoethyl)benzenesulfonyl fluoride, 10 µM pepstatin, 10 µM leupeptin, 10 µM *trans*-epoxysuccinyl-L-leucylamido-(4-guanidino) butane, and 10 µM *N*-tosyl-L-lysine chloromethyl ketone, pH 7.2) containing 2 mg/ml lysozyme. Benzonase® (1 µl/ml) was added, and the bacteria then passed through a French press (SLM-Aminco, Spectometric Instruments) twice at 1,000 p.s.i. The lysate was incubated on ice under agitation for 1 h with an equal volume of silica/silicon carbide (1:1) to remove DNA and RNA fragments. The lysate was then centrifuged at 1,000 × *g* for 5 min and washed two times under the same conditions. The supernatant fractions were combined and centrifuged for 10 min at 14,500 × *g*. The pellet was resuspended in 2 ml of lysis buffer with the aid of a 22-gauge needle. The suspension was diluted 1:1 in OptiPrep (60% iodixanol) and applied as the 30% concentration step of a discontinuous gradient of Optiprep, with 4-ml steps of 24, 28, 30, 35, and 40% iodixanol, diluted in lysis buffer. The gradient was centrifuged at 50,000 × *g* in a Beckman SW 28 rotor for 60 min. The acidocalcisome fraction pelleted at the bottom of the tube and was resuspended in lysis buffer. Gradient fractions and markers were assayed as previously described (23).

Analytical Methods and Immunoblotting—Bacteria were washed once with Dulbecco's PBS, and then PP_i and long chain and short chain polyPs were extracted as described previously (24). Pyrophosphatase activity was assayed by measuring released phosphate using the EnzChek phosphate assay (23, 25). The apparent K_m for PP_i was calculated by using a nonlinear regression program (Sigma Plot 1.0, Jandel Scientific) using the Hill equation. Protein determination was carried out by using the Coomassie Blue protein assay reagent from Bio-Rad. The proteins were separated by SDS-PAGE using 10% gels and then blotted onto nitrocellulose using a Bio-Rad Transblot apparatus. Subsequent processing steps were performed in Dulbecco's PBS containing 0.1% Tween 20. The blots were blocked for 1 h in 5% nonfat dry milk, washed three times, and then incubated with polyclonal antibody 326 against A*rabidopsis* H^+-PPase (20) (1:1,000) for 1 h at room temperature. The blots were then washed three times, incubated for 1 h with horseradish peroxidase-labeled anti-rabbit IgG (1:20,000), washed three times, and processed for chemiluminiscence detection as per the manufacturer's instructions (Amersham Biosciences). Molecular weights were calculated using prestained molecular weight markers.

Immunofluorescence Microscopy—For subcellular localization of H^+-

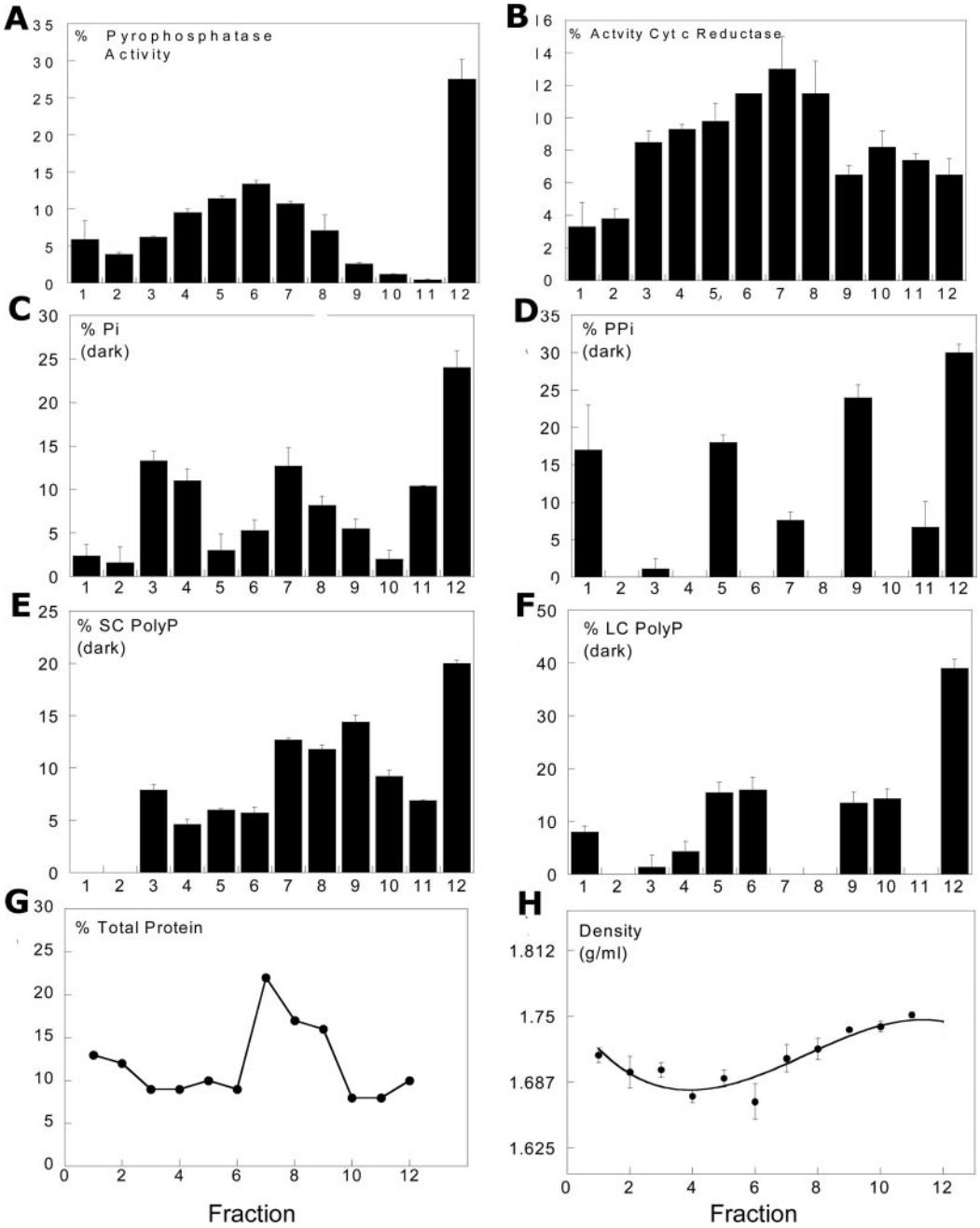

FIG. 3. **Distribution of different markers from *R. rubrum* on iodixanol gradients.** Pyrophosphatase activity (*A*) is concentrated in a distinct dense fraction (fraction 12). This distribution was compared with that of the established plasma membrane marker, succinate cytochrome *c* reductase (*B*). A lower amount of pyrophosphatase activity co-localized with the plasma membrane marker. The *closed circles* in *G* indicate protein distribution in the different fractions and density distribution is shown in *H*. P_i (*C*), PP_i (*D*), and short chain (*SC*, *E*) and long chain (*LC*, *F*) polyPs are also concentrated in fraction 12 (acidocalcisome fraction).

PPase, bacteria were washed with Dulbecco's PBS and fixed in 4% freshly prepared formaldehyde for 10 min at room temperature and 50 min at 4 °C, attached to poly L-lysine treated glass slides, and permeabilized with 0.2% Nonidet P-40 in PBS for 10 min. The samples were blocked for 1 h with PBS containing 3% bovine serum albumin, 1% cold fish gelatin, and 50 mM NH_4Cl and were first incubated for 1 h at room temperature with the polyclonal antibody against the *Arabidopsis thaliana* H^+-PPase (20) or monoclonal antibody against *T. cruzi* H^+-PPase (21), diluted 1: 50 (polyclonal) or 1:100 (monoclonal) in 1% cold fish gelatin. Bacteria were subsequently incubated for 60 min at room temperature with fluorescein-conjugated secondary antibody diluted 1:200 in PBS plus 1% cold fish gelatin. Coverslips were mounted in glass slides with Vectashield® media and sealed. The images were collected with an Olympus laser scanning confocal microscope or an Olympus BX-60 fluorescence microscope.

For polyP localization, bacteria were washed twice with Dulbecco's PBS and resuspended in the same buffer and fixed for 30 min with 4% formaldehyde. 45 μl of this suspension was incubated at room temperature with 10 μg/ml DAPI. After 10 min, the samples were mounted on a slide and observed using the fluorescence microscope (9).

For localization of LysoSensor blue DND-167, bacteria were centrifuged and resuspended in prewarmed (30 °C) Sistrom medium containing 1 μM LysoSensor. Bacteria were incubated for 1 h at 30 °C, centrifuged, and resuspended in fresh prewarmed Sistrom medium. Bacteria were mounted on a slide and observed with the fluorescence microscope using UV excitation. For cycloprodigiosin detection, bacteria were centrifuged, resuspended in Dulbecco's PBS containing 100 nM cycloprodigiosin, and incubated for 30 min. Bacteria were mounted on a slide and observed with the fluorescence microscope using a red emission filter. Bacteria resuspended in Dulbecco's PBS or Sistrom medium, but without cycloprodigiosin or LysoSensor, respectively, were used as controls.

For co-localization studies of chromatophore proteins and H^+-PPase, polyclonal antibodies against crude membranes of phototropic *R. rubrum* cells were adsorbed with *R. rubrum* grown aerobically in the dark,

TABLE I
Cellular content of PP_i and short chain and long chain polyP in R. rubrum

Growth conditions	PP_i	Short chain polyP	Long chain polyP
	μmol/mg protein	*μmol/mg protein*	*μmol/mg protein*
Dark	127 ± 0.5[a]	241 ± 0.6	446 ± 0.3
Light	534 ± 0.2	356 ± 0.18	508 ± 0.12

[a] The values are the means ± S.D. (n = 3).

to remove nonspecific antibodies (22). Cells grown aerobically were fixed with 4% formaldehyde for 1 h followed by permeabilization with 0.3% Triton X-100 in PBS for 10 min and then washed twice with PBS. The cells were then incubated with the antibodies against crude membranes for 45 min at 37 °C and centrifuged, and the antibody that was not adsorbed was collected from the supernatant. For co-localization studies, the cells were incubated 1 h with antibodies diluted 1:20 and with a mouse monoclonal antibody against *T. cruzi* H^+-PPase, diluted 1:50. The cells were subsequently incubated for 60 min at room temperature with rabbit fluorescein-conjugated secondary antibody diluted 1:100 and with mouse rodamine-conjugated secondary antibody diluted 1:200 in PBS plus 1% cold fish gelatin. Control preparations were incubated with preimmune serum or without the primary antibody.

Three-dimensional Confocal Immunofluorescence Microscopy Reconstruction Analysis of H^+-PPase Staining in R. rubrum—Volumetric renderings through a representative bacterial cell were compiled using the average projection ray tracing algorithm (26, 27) in the Olympus FluoView software suite. Further image processing was conducted using the ImageJ software tools and Application Programming Interface originally developed by Wayne Rasband at the National Institutes of Health (rsb.info.nih.gov/ij/). The voxel signal intensities were normalized (28) to enable easier discrimination of relative pixel intensities, and a median filter (28, 29) was applied to correct image artifacts caused by shot noise (30). A Gaussian filter (28, 29) was applied to further counteract image artifacts caused by statistical noise (30), and a colorized lookup table (31) was applied to the 8-bit gray scale image to convey the spectral detection range under which the data was acquired. Average projections through the *xyz* plane and the *zyx* plane were selected to depict the relative signal intensities through the volumetric dataset. *Size bars* and *arrows* were applied as overlays to the *xyz* and *zyx* images using tools in Adobe Photoshop.

Electron Microscopy and X-ray Microanalysis—For routine electron microscopy, bacteria were washed with Dulbecco's PBS and fixed for 1 h with 2.5% grade II glutaraldehyde, 4% freshly prepared formaldehyde, 0.03% $CaCl_2$, and 0.03% picric acid in 0.1 M cacodylate buffer, pH 7.2. Bacteria were post-fixed with OsO_4 for 45 min and then for 15 min with potassium ferricyanide, washed, and treated with 2% uranyl acetate for 30 min. Subsequently, the samples were dehydrated by successive incubations of 6 min with increasing concentrations of ethanol (10, 25, 50, 75, 95, and 100%) at room temperature. Epoxy embedding was carried out by resuspending the sample once in 1:1 ethanol/acetonitrile, twice in 100% acetonitrile, then 30 min in 1:1 Epoxy/acetonitrile, 1.5 h in 3:1 Epoxy/acetonitrile, and 4 h in 100% Epoxy. The embedded samples were polymerized for 20 h at 85 °C. Epoxy blocks were ultrathin-sectioned, the sections were deposited on 300-mesh copper grids, and the grids were stained with uranyl acetate for 30 min and triple lead stain (lead citrate, lead nitrate, and lead acetate) for 1 min.

For immunocytochemistry, bacteria were washed with Dulbecco's PBS and fixed for 1 h at 4 °C in a solution containing 0.5% grade I glutaraldehyde, 4% freshly prepared formaldehyde, 1% picric acid, in 0.1 M cacodylate buffer, pH 7.2. Fixed bacteria were washed with Dulbecco's PBS and dehydrated by successive incubations of 6 min each with increasing concentrations of ethanol (10, 25, 50, 75, 95, 100, and 100%) at −20 °C. The samples were embedded in Unicryl at 4 °C by incubation with 1:1 ethanol/Unicryl for 1 h and 100% Unicryl for 1, 16, and 8 h. The embedded samples were polymerized under UV irradiation at −20 °C for 48 h. Thin sections were collected on 300-mesh nickel grids and blocked for 30 min with PBS containing 0.1% Tween 20 and 0.5% cold fish gelatin (PBS-TW-FG). The grids were incubated for 3 h with a mouse monoclonal antibody against *T. cruzi* H^+-PPase (21) diluted 1:10 in PBS-TW-FG. After washing in PBS-TW-FG, the grids were incubated for 1 h with a 5-nm gold conjugate goat anti-mouse antibody. Subsequently, the grids were washed with PBS and then in distilled water, stained with uranyl acetate and lead citrate. Routine and immunocytochemistry samples were observed with a Hitachi H 600 electron microscope.

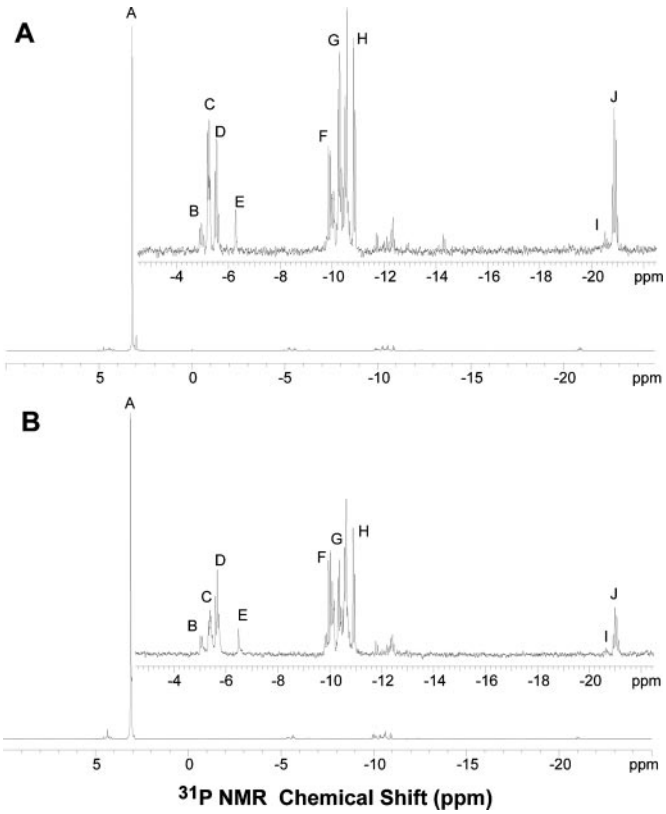

FIG. 4. **303.6 MHz (^{1}H decoupled) ^{31}P NMR spectra of perchloric acid extracts of *R. rubrum* grown under light (*A*) and dark (*B*) conditions.** The *insets* show the upfield region of the spectra (−2.5 to −22.5 ppm) amplified by a factor of 20. Resonance assignments are given in Table II.

For imaging whole bacteria, the preparations were washed in 0.25 M sucrose, and a 5-μl sample was placed on a Formvar-coated 200-mesh copper grid, allowed to adhere for 10 min at room temperature, blotted dry, and observed directly with a Hitachi 600 transmission electron microscope operating at 100 kV (9). Energy-dispersive x-ray analysis was done at the Electron Microscopy Center of Southern Illinois University (Carbondale, IL). The spectra shown are the ones that yielded the most counts in 100 s (of 10 spectra obtained from granules of different bacteria in each preparation), but all other spectra taken from acidocalcisomes of the same preparation were qualitatively similar. Specimen grids were examined in a Hitachi H-7100FA transmission electron microscope at an accelerating voltage of 50 kV. Fine probe sizes were adjusted to cover the electron-dense vacuoles (or a similar area of the background), and x-rays were collected for 100 s by utilizing a thin window (Norvar) detector. Analysis was performed by using a Noran Voyager III analyzer with a standardless analysis identification program.

Perchloric Acid Extracts—For NMR, bacteria were washed twice with buffer A (116 mM NaCl, 5.4 mM KCl, 0.8 mM $MgSO_4$, 50 mM Hepes, pH 7.2) and then extracted with ice-cold 0.5 M $HClO_4$ (2 ml/g wet weight cells). After 30 min of incubation on ice, the extracts were centrifuged at 3,000 × g for 5 min. The supernatants were neutralized by the addition of 0.72 M KOH, 0.6 M $KHCO_3$ (32). Precipitated $KClO_4$ was removed by centrifugation at 12,000 × g for 10 min., the supernatant was separated, and EDTA was added to a final concentration of 100 μM prior to adjusting to pH 8. All of the extracts contained 10% D_2O (v/v) to provide a field frequency lock.

NMR Spectroscopy—Phosphorus NMR spectra were acquired at 303.6 MHz using a Varian INOVA NMR spectrometer equipped with a 17.6 Tesla Oxford Instruments magnet. For perchloric acid extracts, 16,384 transients were collected at room temperature using 25-μs (90°) pulse excitation, 20-kHz spectral width, 32,768 data points, and a 5-s recycle time. Inverse-gated proton decoupling was used to remove nuclear Overhauser effect and J-coupling effects. The chemical shifts of all ^{31}P spectra were referenced to 0 ppm using an 85% phosphoric acid external reference (33). The specific assignments of individual resonances were initially based on published chemical shifts and ^{31}P-^{31}P scalar couplings (33). NMR spectra were processed using the VNMR

6.1B software package (Varian Inc., Palo Alto, CA) running on a Sun Ultra5 (Sun Microsystems, Santa Clara, CA) work station, and included base-line correction, zero filling, and a 3-Hz exponential line broadening prior to Fourier transformation.

RESULTS

Acidocalcisomes are recognizable by their strong electron density when observed by electron microscopy in unfixed and unstained whole cell mounts (6). Using this technique, *R. rubrum* grown in the dark showed both large and small granules, in different locations of the cells (Fig. 1*A*, *arrows*). The large granules have a diameter of ~205 ± 24 nm. X-ray microanalyses were performed on these granules, and a representative spectrum (Fig. 1*B*) shows that the counts for phosphorus were ~3-fold greater than the counts for magnesium, which were approximately the same as the counts for potassium. The counts for oxygen and phosphorus were approximately the same. The medium used to grow *R. rubrum* in the previous experiments was calcium-deficient, which might explain the lack of detectable levels of calcium in the x-ray microanalyses of the acidocalcisomes (Fig. 1*B*). To test this idea, we therefore next cultivated bacteria in the presence of 100 mM $CaCl_2$ for 4 h before preparing them for x-ray microanalysis. Fig. 1*C* shows that there is a dramatic increase in the counts for calcium as well as a decrease in the counts for magnesium and potassium in the acidocalcisomes of these cells. The presence of these elements was not detected in spectra taken from the background (Fig. 1*D*) and demonstrates the ability of acidocalcisomes to accumulate calcium. Peaks for copper and in part for carbon arise from the grid.

Examination of cells in thin sections showed round vacuoles of ~200 nm in cells grown both in the light (Fig. 2*A*, *arrowhead*) and in the dark (Fig. 2*B*, *arrowhead*), clearly different from the chromatophore membranes detected in cells grown in the light (Fig. 2*A*). As is characteristic of the morphology of acidocalcisomes (6), an electron-dense ring was observed surrounding the apparently empty vacuoles (Fig. 2*A*, *arrowhead*). Each intracellular vacuole appeared to be surrounded by a membrane (Fig. 2*B*, *arrowhead*). *R. rubrum* acidocalcisomes (Fig. 2*C*) showed a sponge-like appearance that is also typical of acidocalcisomes in different organisms (6–9).

We purified the acidocalcisomes following a purification procedure used for the isolation of acidocalcisomes from *A. tumefaciens* (9). The distribution of different phosphorus-containing compounds and a plasma membrane marker was compared with that of the established marker for acidocalcisomes, H^+-PPase (Fig. 3). The aminomethylenediphosphonate-sensitive pyrophosphatase activity peaks in two different regions along the gradient. Observation of these fractions by electron microscopy showed that the only fraction containing acidocalcisomes was fraction 12. Fraction 6 was rich in cell ghosts and membranes. The succinate cytochrome *c* reductase, used as a plasma membrane marker, peaks together with the second peak, having pyrophosphatase activity.

R. rubrum contains considerable levels of long and short chain polyP, as measured by determining degradation of polyP with recombinant yeast exopolyphosphatase (24), as well as PP_i (Table I). The acidocalcisome fraction (fraction 12) contained significant amounts (20 and 35%, respectively) of short and long chain polyP, together with considerable amounts of P_i and PP_i (25 and 30%, respectively). These results suggest preferential acidocalcisomal localization of these compounds.

Fig. 4 shows the 303.6 MHz (^{1}H decoupled) ^{31}P NMR spectra of *R. rubrum* grown under light (Fig. 4*A*) and dark (Fig. 4*B*) conditions. Resonance assignments for these spectra are given in Table II. The dominant peak in all spectra is inorganic phosphate (*peak A*). The *insets* of Fig. 4 are the upfield regions of the spectra (2.5 to −22.5 ppm) magnified 20× respective to the overall spectra. The region between −4 and −6.5 ppm contains peaks for the terminal phosphates of nucleotide di- and triphosphates (*peaks D* and *C*, respectively) in addition to a peak for the terminal phosphates of polyphosphates (*peak B*) and a peak for pyrophosphate (*peak E*). The region from −9 to −11 ppm contains peaks for the α-phosphates of nucleotide di- and triphosphate (*peaks F* and *G*, respectively) as well as peaks for NAD (*peak H*). The most upfield parts of the spectra contain peaks from the β-phosphate of nucleotide triphosphate (*peak J*) and peaks for the β-phosphates of tri- and tetrapolyphosphates (*peak I*). The main difference between the bacteria grown under light and dark conditions is that those grown in the dark contain less nucleotide triphosphates (*peak J*), pyrophosphate (*peak E*), and polyphosphate (*peaks B* and *I*).

To confirm the acidocalcisomal localization of polyP, we detected it using DAPI, which as reported previously, can be used

TABLE II
^{31}P NMR resonance assignments for perchloric acid extracts of R. rubrum
Published assignments for *T. cruzi* are provided for comparison.

Peak	Assignment	*R. rubrum*		*T. cruzi*[a]
		Light	Dark	
A	Inorganic phosphate	2.60	2.62	2.65
B	α-P of polyphosphates	−4.98	−5.01	−5.52
C	γ-P of NTP	−5.33	−5.33	ND[b]
D	β-P NDP	−5.57	−5.64	−5.93
E	Pyrophosphate	−6.28	−6.32	−6.95
F	α-P of NDP	−9.90	−9.95	−10.60
G	α-P of NTP	−10.32	−10.36	−10.97
H	NAD(H)	−10.79	−10.90	−11.22
I	β-P of tri- and tetrapolyphosphates	−20.51	−20.60	−20.89
J	β-P of NTP	−20.91	−20.98	−21.33
K	Central P of long chain polyphosphates	ND	ND	−21.58

[a] Ref. 32.
[b] ND indicates that the peak was not detected.

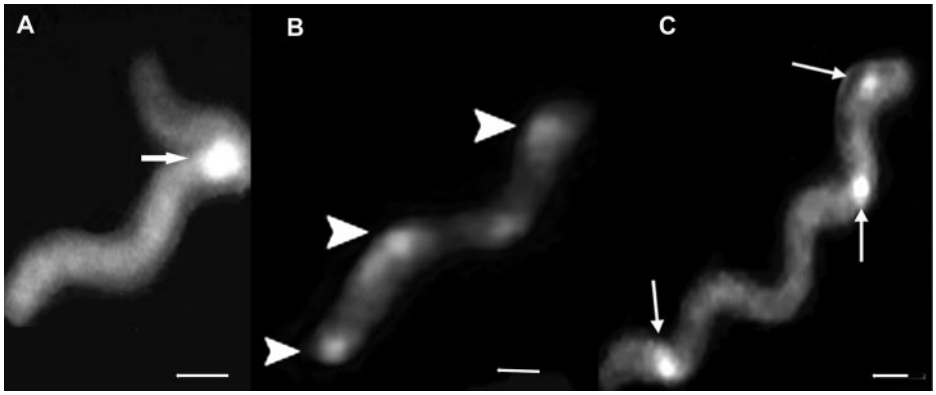

FIG. 5. **Identification of acidocalcisomes of *R. rubrum*.** Staining of acidocalcisomes with DAPI (*A*), LysoSensor (*B*), and cycloprodigiosin (*C*). The cells were incubated as described under "Experimental Procedures" and observed by fluorescence microscopy. Note the staining (*arrows* and *arrowheads*). *Bars*, 0.5 μm.

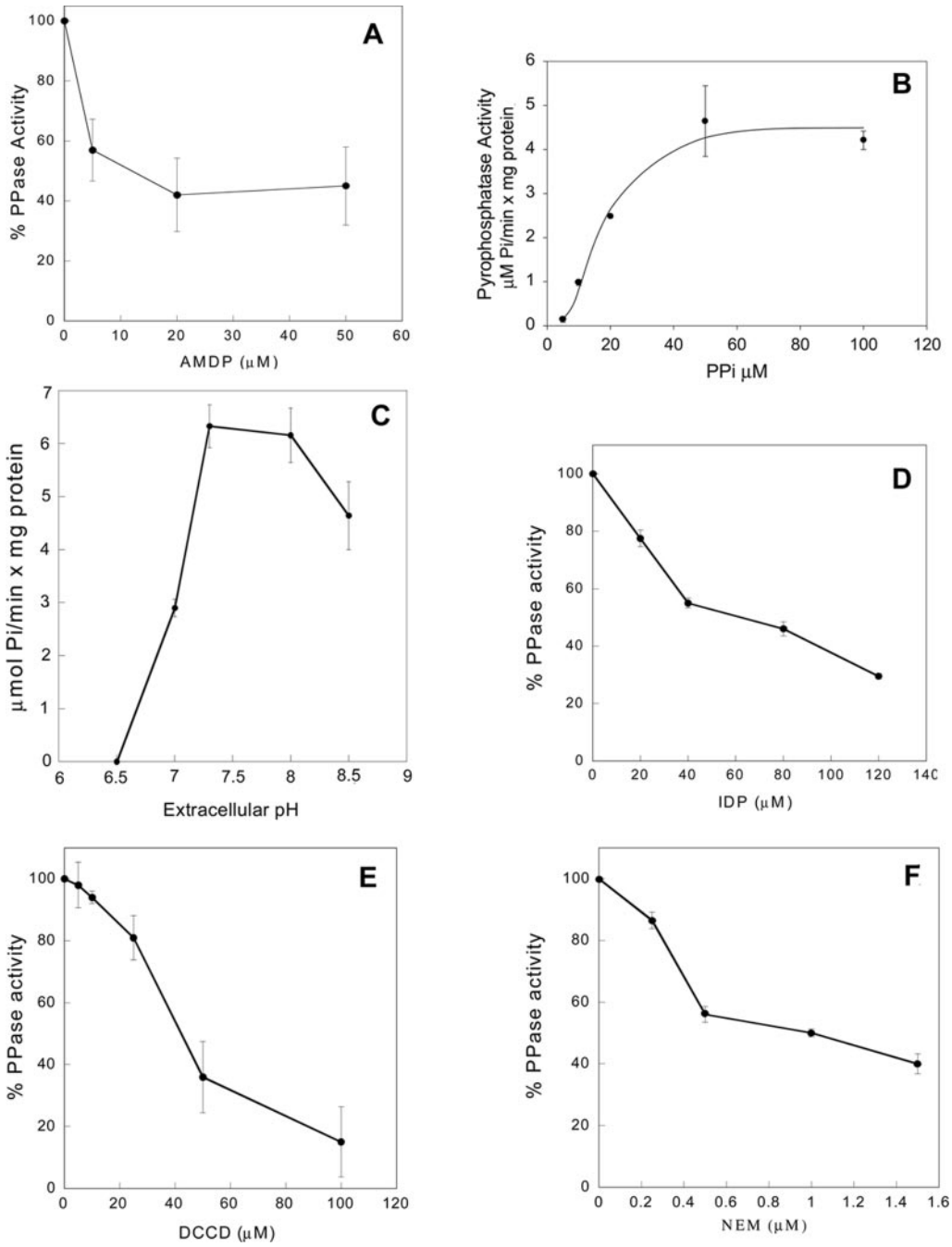

FIG. 6. **Characterization of acidocalcisome pyrophosphatase.** Shown are the effect of AMDP (*A*), the initial rate of pyrophosphate hydrolysis as a function of pyrophosphate concentration (*B*) and medium pH (*C*), and the effects of IDP (*D*), DCCD (*E*), and *N*-ethylmaleimide (*F*). Aliquots of the acidocalcisome fraction were added to a standard reaction mixture (*B* and *C*) in the presence of increasing concentrations of pyrophosphate (*B*) or incubated in the standard reaction mixture adjusted to different pH values (*C*). Aliquots of acidocalcisomes were added to the standard reaction mixture in the presence of increasing concentrations of AMDP (*A*), IDP (*D*), DCCD (*E*), or *N*-ethylmaleimide (*F*). The percentage of inhibition compared with the control in the absence of inhibitors (100%) is indicated. Control activities were 0.74 ± 0.04 μmol of PP_i consumed/min × mg protein. The *error bars* indicate the S.E. of the mean values from at least three separate experiments.

for the cytochemical detection of this inorganic polymer (24). Fig. 5*A* shows labeling of acidocalcisomes with DAPI. As occurs with acidocalcisomes from *A. tumefaciens* (9), and other organisms (6), the organelles from *R. rubrum* could also accumulate dyes used to detect acidic compartments, such as Lysosensor Blue DND-167 (Fig. 5*B*), and cycloprodigiosin (Fig. 5*C*). Cycloprodigiosin is a compound isolated from a marine bacterium that has been shown to uncouple H^+-PPase activity acting as a chloride/proton symport (34) and has been shown to stain acidocalcisomes of *T. cruzi* (23). Based on the positive staining with Lysosensor blue DND-167, which has been used to detect very acidic intracellular compartments (35), we can estimate a very low pH in *R. rubrum* acidocalcisomes (pH ~5–5.5).

Acidification of acidocalcisomes takes place in most organisms by the action of a membrane-bound H^+-PPase (6). The pyrophosphatase activity detected in the acidocalcisome fraction of *R. rubrum* (Fig. 6*A*), as measured by inorganic phosphate detection (25), was 0.73 ± 0.04 μmol of pyrophosphate consumed/min × mg protein (means ± S.E. of results from three separate experiments) and was partially (60%) inhibited by 20–50 μM AMDP, a specific inhibitor of H^+-PPases (36). The lack of complete inhibition suggests the presence of another pyrophosphatase activity in the acidocalcisome fraction. In this regard, it has recently been reported that *Trypanosoma brucei*

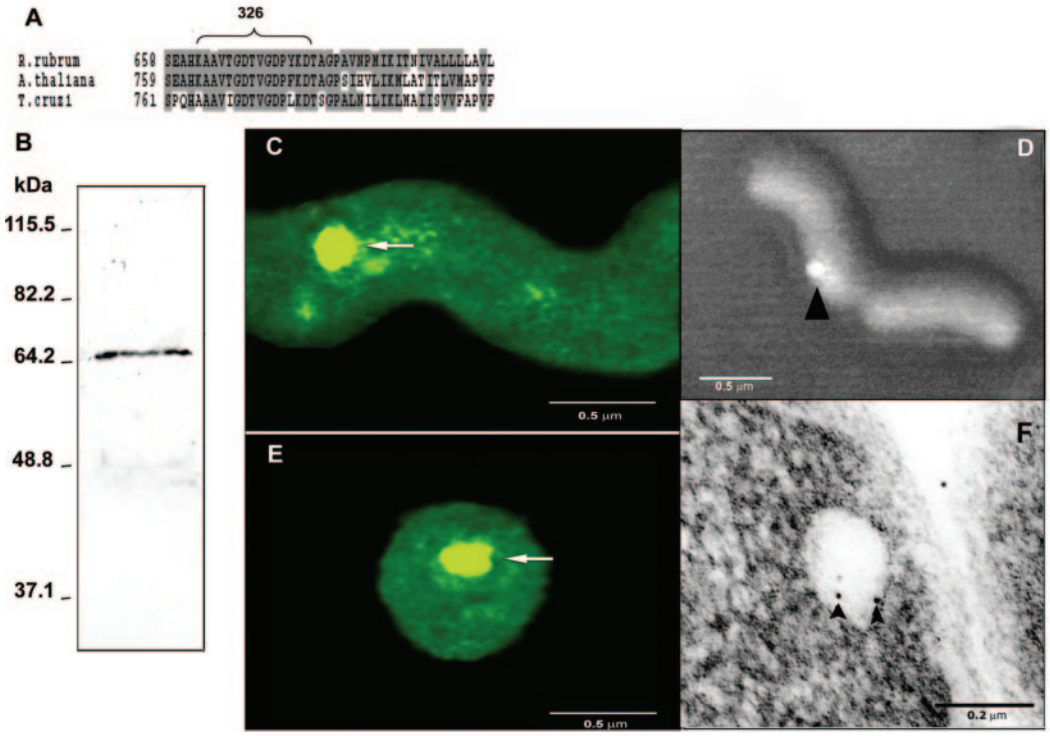

FIG. 7. **Western blot analysis, immunofluorescence analysis, and immunoelectron microscopy of H^+-PPase in *R. rubrum*.** *A*, CLUSTAL W alignment of the C-terminal region of H^+-PPases from *R. rubrum* (GenBank™ accession number AAC38615), *A. thaliana* (GenBank™ accession number BAA32210), and *T. cruzi* (GenBank™ accession number AF159881). Homologous residues are *shaded*. *B*, detection of the H^+-PPase by immunoblot, using polyclonal antibody against the *A. thaliana* H^+-PPase. *R. rubrum* proteins (33 μg) were separated by SDS-PAGE and transferred to nitrocellulose. The immunoblot probed with antibody against the H^+-PPase recognized a polypeptide of apparent molecular mass of 65 kDa. *C* and *E*, three-dimensional confocal immunofluorescence microscopy reconstruction analysis of the H^+-PPase of *R. rubrum* as seen in a parallel (*C*) or transverse (*E*) view. The *arrows* show labeling of acidocalcisomes. *D*, confocal fluorescence image overlaid on bright field image of the same cell. *Bars*, 0.5 μm. *F*, immunoelectron microscopy of the cells. Labeling of an acidocalcisome is evident (*arrowheads*). *Bar*, 0.2 μm.

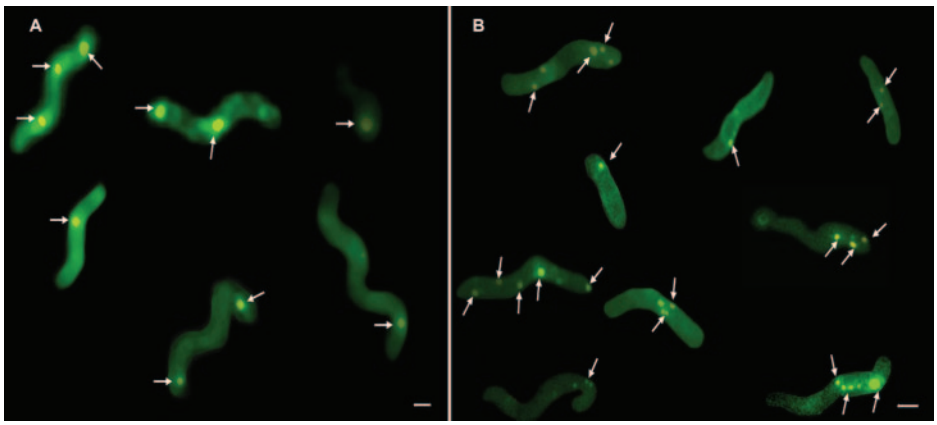

FIG. 8. **Confocal immunofluorescence analysis of *R. rubrum* grown in dark (*A*) and light (*B*) conditions.** Note the larger number of acidocalcisomes in cells grown under light conditions (*B*). Immunofluorescence analysis was done as for Fig. 7*D*. *Bar*, 0.5 μm.

acidocalcisomes possess an inorganic pyrophosphatase, in addition to the H^+-PPase (37). The presence of a soluble pyrophosphatase in *R. rubrum* has also been reported (38). The dependence of the initial rate of hydrolysis on pyrophosphate concentration in *R. rubrum* acidocalcisome fractions is shown in Fig. 6*B*. Activity was maximal at ~60 μM pyrophosphate with an apparent K_m of 17.8 μM. Fig. 6*C* shows the effect of pH on the initial rate of pyrophosphate hydrolysis in the *R. rubrum* acidocalcisome fraction. Activity was optimal at pH 7.5–8.0, and potassium-insensitive as reported previously (39). Pyrophosphate hydrolysis of the acidocalcisome fraction was inhibited, in a dose-dependent manner, by the pyrophosphate analog IDP (Fig. 6*D*). Fig. 6 also shows that dicyclohexylcarbo-diimide (DCCD) (Fig. 6*E*) and the thiol reagent *N*-ethylmaleimide (Fig. 6*F*) were also effective in inhibiting the *R. rubrum* pyrophosphatase activity in a dose-dependent manner, as has been reported before in other studies of this enzyme (39). Taken together, these results indicate that the pyrophosphatase activity identified in acidocalcisomes has similar characteristics to the H^+-PPase activity detected previously in *R. rubrum*.

We also investigated the localization of the H^+-PPase by immunocytochemistry using an antibody (20) against a peptide of *A. thaliana* H^+-PPase (326) that is conserved in the C-terminal region of the *R. rubrum* sequence available in GenBank™ (accession number AAC38615; Fig. 7*A*). This antibody showed cross-reactivity with a band of 65 kDa present in the *R. rubrum* acidocalcisome fraction (Fig. 7*B*). No background staining was observed when preimmune serum was used as a control (data not shown). Immunofluorescence microscopy using these antibodies resulted in staining of acidocalcisomes

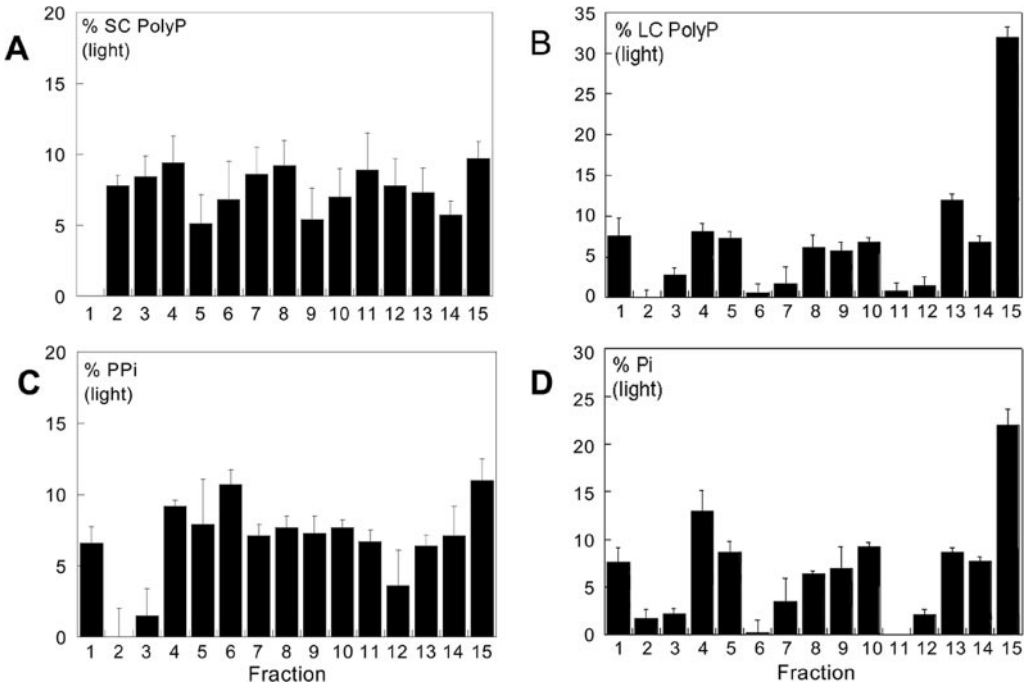

FIG. 9. **Distribution of phosphorus-containing compounds from *R. rubrum* grown under light.** Short chain (*SC*, *A*) and long chain (*LC*, *B*) polyP, PP_i (*C*), and P_i (*D*) concentrated in the highest density iodixanol gradient fraction (fraction 15), which contains the acidocalcisomes. The methods as for Fig. 3.

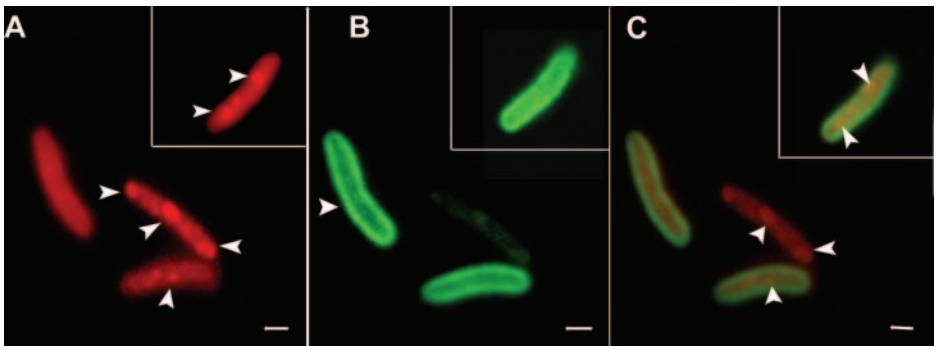

FIG. 10. **Confocal immunofluorescence analysis of chromatophore proteins and H^+-PPase in *R. rubrum*.** *A* shows staining with antibodies against the H^+-PPase, *B* shows staining by antibodies previously adsorbed with lysates of *R. rubrum* grown under anaerobic conditions, and *C* shows the overlay. *Bars*, 0.5 μm.

(Fig. 7, *C–E*, *arrows* and *arrowhead*), at the same position where the organelles were located by direct transmission electron microscopy (Fig. 1*A*) or by LysoSensor (Fig. 5*B*), cycloprodigiosin A (Fig. 5*C*), and DAPI (Fig. 5*A*) staining. These results are in agreement with the co-localization of polyP and the pyrophosphatase in the acidocalcisomes as assayed biochemically (Fig. 3). Immunoelectron microscopy confirmed labeling in vacuoles with an "empty" appearance (Fig. 7*F*, *arrowheads*). Volumetric rendering of the image shown in Fig. 7*C* showed the predominant acidocalcisome localization of the H^+-PPase (see movie in the supplemental material).

When *R. rubrum* cells were grown in the light (Fig. 8*B*), there were more acidocalcisomes detected by staining with monoclonal antibodies against the *T. cruzi* H^+-PPase than found in cells grown in the dark (Fig. 8*A*). There were 3.3 ± 0.2 acidocalcisomes/cell under light conditions and 2.1 ± 0.1 acidocalcisomes/cell under dark conditions ($n = 49$; $p < 0.05$). Subcellular fractionation of *R. rubrum* grown in the light showed a similar distribution of P_i, PP_i, and short and long chain polyP (Fig. 9) as shown in cells grown in the dark (Fig. 3), except that lower percentages of PP_i and short chain polyP were detected in the acidocalcisomal fractions (fraction 15 in these gradients).

R. rubrum H^+-PPase was originally detected in chromatophores obtained after sonication and differential centrifugation. However, immunolocalization studies to determine its localization in the chromatophore membranes have not been reported previously. We therefore investigated whether the H^+-PPase co-localized with the photosynthetic apparatus of *R. rubrum* that is known to be located in the plasma and chromatophore membranes of the bacterium. As a marker of the photosynthetic apparatus, we incubated bacteria grown in the dark with antibodies developed against whole bacteria grown in the light to adsorb nonspecific antibodies (22) and then used the supernatants as specific antibodies against the photosynthetic apparatus in co-localization studies. Fig. 10*A* shows that antibodies against the H^+-PPase stain predominantly the acidocalcisomes with a diffuse staining of the cytosol. An increase in the concentration of the antibody did not increase the staining of the plasma membrane. Antibodies against the photosynthetic apparatus stain mainly the plasma membrane and regions adjacent to it (Fig. 10*B*). A yellowish color in the plasma membrane of overlays suggested some co-localization, although most structures showed distinct staining (Fig. 10*C*).

DISCUSSION

The H^+-PP synthase/H^+-PPase was first described in chromatophores from *R. rubrum* (10, 11) where it was shown to

catalyze light-induced formation of PP_i from P_i or the reverse hydrolysis of PP_i to P_i. Proton movement, which was induced by light in chromatophores (40), was shown by addition of PP_i in the dark to be linked also to the H^+-PPase (41).

Chromatophores are a particulate fraction obtained after sonication of several purple bacteria (42). Their counterparts in the intact bacteria are known as chromatophore membranes. The apparent continuity between the chromatophore and plasma membranes has led to the hypothesis that chromatophore membranes are formed by invagination of the plasma membrane (22), and this has been supported by freeze etching studies in *R. rubrum* (43). Interestingly, freeze etching studies of *R. rubrum* (44) have also revealed the presence of large membrane-bound vesicles very similar in size to the acidocalcisomes described in this work (Fig. 2). Because the H^+-PPase was found in chromatophores, it was argued that the enzyme physiologically pumps protons across the plasma membrane and that the plasma membrane is its usual environment (15, 38). Our results indicate that the H^+-PPase of *R. rubrum* is predominantly located in an intracellular compartment, similar to the acidocalcisome of *A. tumefaciens* (9) and unicellular eukaryotes (6), where it might be responsible for its acidification. These results also provide further evidence for the presence of acidocalcisomes, defined as acidic organelles rich in PP_i, polyP, calcium, and other elements, in another prokaryote distantly related to *A. tumefaciens*.

Although our results provide strong evidence for a predominant acidocalcisomal location of the H^+-PPase, previous biochemical experiments have shown that the H^+-PPase is able to synthesize PP_i when an electrochemical H^+ gradient is formed across the chromatophore membrane upon illumination (10, 15), providing support for an additional plasma membrane/chromatophore membrane location. This is a similar situation to what has been described in eukaryotes, where the H^+-PPase is present in several locations, such as, for example, vacuolar and plasma membranes of pea cotyledons (13) and contractile vacuole (7, 46) and acidocalcisomes (7) of *C. reinhardtii*. However, the H^+-PPase could be used as a marker of acidocalcisomes, not because is absent in other locations but because it is highly concentrated in them (6).

The results presented in this work are also in agreement with a recent report (47) that showed a higher expression of the H^+-PPase in cells grown anaerobically in the light than in cells grown in the dark in aerobic cultures not subjected to intense agitation.

Because *R. rubrum* apparently possesses only one gene for the H^+-PPase (48), our results invalidate the distinction between vacuolar (V-H^+-PPase) and nonvacuolar (H^+-PPase) enzymes based solely on their localization in vacuoles (tonoplasts and acidocalcisomes) or bacterial plasma membranes (49). A more appropriate classification based on phylogenetic analyses of a large set of H^+-PPase sequences separates H^+-PPases into K^+-dependent and K^+-independent (39, 50–52) forms. *R. rubrum* and *A. tumefaciens* (9) H^+-PPases are K^+-independent enzymes, and as with the enzyme from *A. tumefaciens* (9), the H^+-PPase from *R. rubrum* is also sensitive to inhibition by aminomethylenedisphosphonate, imidodiphosphate, DCCD, and *N*-ethylmaleimide but has only a low sensitivity to the soluble PPase inhibitor, fluoride (Fig. 5 and Ref. 39).

It has been reported that in *R. rubrum* PP_i can be as high as 43 mM in illuminated cells and that most of this PP_i is in the form of granules (18, 45). In agreement with these results, we detected larger quantities of PP_i, and short chain polyP (Table I) and a larger number of acidocalcisomes (Fig. 8) in illuminated cells.

In conclusion, the H^+-PPase of *R. rubrum* is located not only in the plasma membrane where it can function in PP_i synthesis but also in the acidocalcisomes where it can act as a proton pump resulting in their acidification.

Acknowledgments—We thank Arthur Kornberg for *E. coli* CA38 pTrcPPX1, Hajime Hirata for cycloprodigiosin, Michael Martin for AMDP, Mary Lynne Perille Collins for antibodies against phototropic cells, John Bozzola and Steve Schmitt for help with the x-ray microanalysis, and Karl Garsha and the Imaging Technology Group at the University of Illinois at Urbana-Champaign for help with the fluorescence microscopy.

REFERENCES

1. Lundin, M., Deopujari, S. W., Lichko, L., Pereira da Silva, L., and Baltscheffsky, H. (1992) *Biochim. Biophys. Acta* **1098,** 217–223
2. Pereira da Silva, L., Sherman, M., Lundin, M., and Baltscheffsky, H. (1993) *Arch. Biochem. Biophys.* **30,** 310–313
3. Vianello, A., Zancani, M., Casolo, V., and Macri, F. (1997) *Plant Cell Physiol.* **38,** 87–90
4. Rea, P. A., and Poole, R. J. (1993) *Annu. Rev. Plant Physiol. Plant Mol. Biol.* **4,** 157–180
5. Zhen, R.-G., Kim, E. J., and Rea, P. A. (1997) *Adv. Bot. Res.* **25,** 297–337
6. Docampo, R., and Moreno, S. N. J. (2001) *Mol. Biochem. Parasitol.* **114,** 151–159
7. Ruiz, F. A., Marchesini, N., Seufferheld, M., Govindjee, and Docampo, R. (2001) *J. Biol. Chem.* **276,** 46196–46203
8. Marchesini, N., Ruiz, F. A., Vieira, M., and Docampo, R. (2002) *J. Biol. Chem.* **277,** 8146–8153
9. Seufferheld, M., Viera, M. C. F., Ruiz, F. A., Rodrigues, C. O., Moreno, S. N. J., and Docampo, R. (2003) *J. Biol. Chem.* **278,** 29971–29978
10. Baltscheffsky, H., Von Stedingk, L.-V., Heldt, H.-W., and Klingenberg, M. (1966) *Science* **153,** 1120–1122
11. Baltscheffsky, M. (1967) *Nature* **216,** 241–243
12. Long, A. R., Williams, L. E., Nelson, S. J., and Hall, J. L. (1995) *J. Plant Physiol.* **146,** 629–638
13. Robinson, D. G., Haschke, H.-P, Hinz, G., Hoh, B., Maeshima, M., and Marty, F. (1996) *Planta* **198,** 95–103
14. Martinez, R., Wang, Y., Benaim, G., Benchimol, M., de Souza, W., Scott, D. A., and Docampo, R. (2002) *Mol. Biochem. Parasitol.* **120,** 205–213
15. Baltscheffsky, M., Schultz, A., and Baltscheffsky, H. (1999) *FEBS Lett.* **457,** 527–533
16. Meyer, A. (1904) *Bot. Zeit.* **62,** 113–152
17. Kornberg, A. (1995) *J. Bacteriol.* **177,** 491–496
18. Salih, G. F., and Nyrén, P. (1990) *Curr. Res. Photosynth.* **3,** 209–212
19. Sistrom W. R. (1960) *J. Gen. Microbiol.* **22,** 778–785
20. Zhen, R.-G., Kim, E. J., and Rea P. A. (1997) *J. Biol. Chem.* **272,** 22340–22348
21. Luo, S., Vieira, M., Graves, J., Zhong, L., and Moreno, S. N. J. (2001) *EMBO J.* **20,** 55–64
22. Crook, S.M., Treml, S. B., and Collins, M.L.P. (1986) *J. Bacteriol.* **167,** 89–95
23. Scott, D. A., and Docampo, R. (2000) *J. Biol. Chem.* **275,** 24215–24221
24. Ruiz, F. A., Rodrigues, C. O., and Docampo, R. (2001) *J. Biol. Chem.* **276,** 26114–26121
25. Scott, D. A., de Souza, W., Benchimol, M., Zhong, L., Lu, H.-G., Moreno, S. N. J., and Docampo, R. (1998) *J. Biol. Chem.* **273,** 22151–22158
26. Drebin, R. Carpenter, L., and Hanrahan, P. (1988) *Proceedings of the 15th Annual Conference on Computer Graphics and Interactive Techniques*, pp. 65–74, ACM Press, New York
27. Meissner, M. Huang, J. Bartz, D., Mueller, K., and Crawfis, R. (2000) *Proceedings of the 2000 IEEE Symposium on Volume Visualization*, pp. 81–91, ACM Press, New York
28. Russ, J. C. (1995) *The Image Processing Handbook*, 2nd Ed., pp. 151–210, CRC Press Inc., Boca Raton, FL
29. van Kempen, G. M. P., van Vliet, L. J., and Verveer, P. J. (1997) in *3-D Microscopy: Image Aquisition and Processing IV* (Cogswell, C. J., Conchello, J.-A., and Wilsonm, T., eds) pp. 114–124, SPIE International Society for Optical Engineering, Bellingham, WA
30. Russ, J. C. (1995) *The Image Processing Handbook*, 2nd Ed., pp. 1–76, CRC Press Inc., Boca Raton, FL
31. Pawley, J. B. (1994) in *Three Dimensional Confocal Microscopy: Investigation of Biological Specimens* (Stevens, J. K., Mill, L. R., and Trogadis, J. E., eds) pp. 47–93, Academic Press, London
32. Moreno, B., Urbina, J. A., Oldfield, E., Bailey, B. N., Rodrigues, C. O., and Docampo, R. (2000) *J. Biol. Chem.* **275,** 28356–28362
33. Van Wazer, J. R., and Ditchfield, R. (1987) in *Phosphorus NMR in Biology* (Burt, C. T., ed) pp. 1–23, CRC Press, Boca Raton, FL
34. Maeshima, M., Nakayasu, T., Kawauchi, K., Hirata, H., and Shimmne, T. (1999) *Plant Cell Physiol.* **40,** 439–442
35. Lin, H.-J, Herman, P., Kang, J. S., and Lakowicz, J. R. (2001) *Anal. Biochem.* **294,** 118–125
36. Zhen, R.-G., Baykov, A. A., Bakuleva, N. P., and Rea, P.A. (1994) *Plant Physiol.* **104,** 153–159
37. Lemercier, G., Espiau, B., Ruiz, F. A., Vieira, M., Luo, S., Baltz, T., Docampo, R., and Bakalara, N. (2004) *J. Biol. Chem.* **279,** 3420–3425
38. Romero, I., Garcia-Contreras, R., and Celis, H. (2003) *Arch. Microbiol.* **179,** 377–380
39. Belogurov, G. A., Turkina, M. V., Penttinen, A., Huopalahti, S., Baykov, A. A., and Lahti, R. (2002) *J. Biol. Chem.* **277,** 22209–22214
40. von Stedingk, L.-V., and Baltscheffsky, H. (1966) *Arch. Biochem. Biophys.* **40,** 400–404
41. Moyle, J., Mitchell, R., and Mitchell, P. (1972) *FEBS Lett.* **23,** 233–236

42. Cohen-Bazire, G. (1963) in *Bacterial Photoshynthesis* (Gest, H., San Pietro, A., and Venon, L. P., eds) pp. 89–110, The Antioch Press, Yellow Spring, OH
43. Oelze, J., and Drews, G. (1972) *Biochim. Biophys. Acta* **265,** 209–239
44. Crofts, A. R. (1970) in *Electron Transport and Energy Conservation* (Tager, J M., Papa, S., Quagliarello, E., and Slater, E. C., eds) pp. 221–228, Adriatica Editrice, Bari, Italy
45. Schultz, A., and Baltscheffsky, M. (2003) *Biochim. Biophys. Acta* **1607,** 141–151
46. Robinson, D. G., Hoppenrath, M., Oberbeck, K., and Ratajczak, R. (1998) *Bot. Acta* **111,** 108–122
47. López-Marqués, R. L., Perez-Castiñeira, J. R., Losada, M., and Serrano, A. (2004) *J. Bacteriol.* **186,** 5418–5426
48. Baltscheffsky, M., Nadanaciva, S., and Schultz, A. (1998) *Biochim. Biophys. Acta* **1364,** 301–306
49. Drozdowicz, Y. M., and Rea, P. A. (2001) *Trends Plant Sci.* **6,** 206–211
50. Perez-Castiñeira, J. R., Lopez-Marques, R. L., Losada, M., and Serrano, A. (2001) *FEBS Lett.* **496,** 6–11
51. Perez-Castiñeira, J. R., Alvar, J., Ruiz-Perez, L. M., and Serrano, A. (2002) *Biochem. Biophys. Res. Commun.* **294,** 567–573
52. Belogurov, G. A., and Lahti, R. (2002) *J. Biol. Chem.* **277,** 49651–49654